HHS Public Access

Author manuscript

Mol Cancer Res. Author manuscript; available in PMC 2020 August 01.

Published in final edited form as:

Mol Cancer Res. 2020 February ; 18(2): 311–323. doi:10.1158/1541-7786.MCR-19-0594.

miR-29a is repressed by MYC in pancreatic cancer and its restoration drives tumor suppressive effects via downregulation of LOXL2

Shatovisha Dey[1], **Jason J. Kwon**[1], **Sheng Liu**[1], **Gabriel A. Hodge**[1], **Solaema Taleb**[1], **Teresa A. Zimmers**[2,3], **Jun Wan**[1,2], **Janaiah Kota**[1,2,*]

[1]Department of Medical and Molecular Genetics, Indiana University School of Medicine, Indianapolis, IN, USA

[2]The Melvin and Bren Simon Cancer Center, IUSM, Indianapolis, IN, USA

[3]Department of Surgery, Indiana University School of Medicine, Indianapolis, IN, USA

Abstract

Pancreatic ductal adenocarcinoma (PDAC) is an intractable cancer with a dismal prognosis. MicroRNA-29a (miR-29a) is commonly downregulated in PDAC, however, mechanisms for its loss and role still remain unclear. Here we show that in PDAC, repression of miR-29a is directly mediated by MYC via promoter activity. RNA-seq analysis, integrated with miRNA target prediction, identified global miR-29a downstream targets in PDAC. Target enrichment coupled with gene ontology and survival correlation analyses identified the top five miR-29a downregulated target genes (LOXL2, MYBL2, CLDN1, HGK and NRAS) that are known to promote tumorigenic mechanisms. Functional validation confirmed that upregulation of miR-29a is sufficient to ablate translational expression of these five genes in PDAC. We show that the most promising target among the identified genes, LOXL2, is repressed by miR-29a via 3'-UTR binding. Pancreatic tissues from a PDAC murine model and patient biopsies showed overall high LOXL2 expression with inverse correlations with miR-29a levels. Collectively, our data delineate an anti-tumorigenic, regulatory role of miR-29a, and a novel MYC-miR-29a-LOXL2 regulatory axis in PDAC pathogenesis, indicating the potential of the molecule in therapeutic opportunities.

Implications—This study unravels a novel functional role of miR-29a in PDAC pathogenesis, and identifies a MYC-miR-29a-LOXL2 axis in regulation of the disease progression, implicating miR-29a as a potential therapeutic target for PDAC.

Graphical Abstarct

*Correspondence to: Janaiah Kota, Ph.D., 975 West Walnut Street, IB 244C, Indianapolis, IN 46202-5251, Phone: (317) 278-2105, Fax: (317) 274-2293, jkota@iu.edu.

Conflict of Interest: The authors declare no potential conflicts of interest.

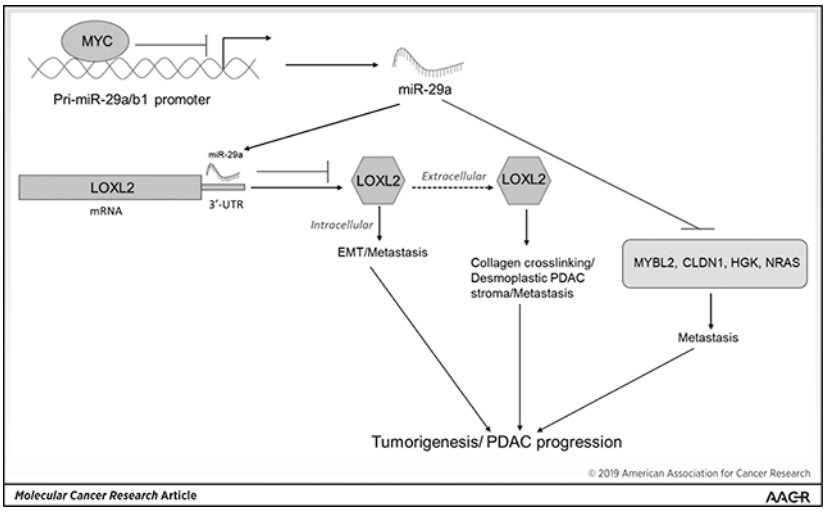

Keywords

microRNA; miR-29a; pancreatic cancer; RNA-seq; LOXL2

Introduction

Pancreatic Ductal Adenocarcinoma (PDAC) is one of the most deadly forms of human malignancies. Being the fourth most lethal cancer in the United States, PDAC accounts for 7% of all estimated cancer-related deaths (1). With an overall 5-year survival rate of less than 5% worldwide (2), the trend for PDAC is projected to worsen over the next decade, rendering PDAC the second leading cause of cancer-related deaths by 2030 (3). Due to lack of efficient biomarkers, PDAC remains undetected till an advanced, metastatic stage when the cancer is aggressive and resistant to current forms of therapeutic modalities (4). Therapeutic failure for PDAC can be attributed to the unique heterogeneous, immune-suppressive tumor microenvironment, which interferes with drug efficacy and cytotoxic T-cell infiltration in the cells (4,5). Over 90% of PDAC cases exhibit driver oncogenic *Kras* mutations with initiation of precursor, pancreatic intraepithelial neoplasia (PanIN) lesions, which lead to aggressive metastatic PDAC (6). Although mutational spectrum of PDAC has been well characterized (6–8), the knowledge is yet to yield effective targeted therapies. Further, there was no success with targeting Kras (9,10) or finding potent Kras inhibitors (11). Thus, there is a crucial need for investigating the molecular mechanisms of PDAC to identify *de novo* targets for the disease aimed at developing effective therapeutic strategies to prolong life expectancies of PDAC patients.

MicroRNAs (miRNAs) play pivotal roles in regulating a broad array of biological processes related to cancer pathogenesis (12). Particularly, studies have shown tumor suppressor miRNAs to be repressed in a wide variety of cancer types, which in turn, de-repress proto-oncogenic factors promoting cancer phenotypes (12). In our previous reports, we demonstrated the pathological role of microRNA-29a (miR-29a) in PDAC tumor-stromal biology (13,14). We found miR-29a to remain downregulated in pancreatic cancer cells

(PCCs) and associated fibroblasts (13,14). However the mechanisms of miR-29a downregulation and its downstream effectors in PDAC is still unclear. The current study delineates the upstream regulation of miR-29a in PDAC and characterizes global miR-29a targetome in the disease. Here we reveal for the first time, the association of miR-29a-LOXL2 axis is regulation of PDAC pathogenesis.

Materials and Methods

Accession Number

The RNA-seq data reported in this study is available at the GEO database under the accession number GSE128663.

Experimental Mice

$Kras^{LSL.G12D/+}$; $p53^{LSL.R172H/+}$ (KP) mice were generated and crossed with Pdx1-Cre mice to obtain the $Kras^{LSL.G12D/+}$; $p53^{R172H/+}$; Pdx1-Cre (KPC) mice used in this study. All animal protocols were reviewed and approved by the Indiana University Animal Care and Use Committee. Regulatory guidelines set by Guide for the Care and Use of Laboratory Animals of the National Institute of Health were followed for all animal housing, use and euthanasia procedures.

Patient Tissue Procurement

This study was reviewed and approved by the Indiana University (IU) Institutional Review Board (IRB) (IU IRB # 1312935090R004). Patient tissues were obtained as described previously (13).

Cell Culture

Normal human pancreatic epithelial cell lines HPNE (CRL-023, ATCC) and HPDE (T0018001, AddexBio), and PCC lines Panc-1 (CRL-1469, ATCC) and MIA PaCa-2 (CRL-1420, ATCC) were cultured in Dulbecco's Modified Eagle Medium (DMEM) (11965092, Life Technologies) supplemented with 10% FBS. AsPC-1 (CRL-1682, ATCC) and BxPC-3 (CRL-1687, ATCC) PCC lines were grown in RPMI 1640 medium (11875–093, Gibco™) supplemented with 10% FBS. Cells were grown in a humidified 5% CO_2 incubator at 37°C. Cell lines were authenticated by morphologic inspection and mycoplasma testing. Experiments were performed with cells of passage of <10.

RNA Extraction

Total RNA was extracted from cultured cells or frozen pancreatic tissues using Trizol Reagent (Invitrogen™). The concentration and purity of the extracted RNAs were measured using a Nanodrop 2000 Spectrophotometer (Thermo Fisher Scientific) and stored at −80°C for future use.

Quantitative Real time PCR (qRT-PCR)

RNA was reverse transcribed to generate cDNA using High capacity cDNA Reverse Transcription kit (4368814, Thermo Fisher Scientific) with random primers or custom

primer pool for miRNA (Applied Biosystems). miRNA and LOXL2 expressions were measured using TaqMan Assays. Other gene expressions were measured using SYBR Green assays with primers shown in Supplementary Table S1. Primary (pri)-miR-29a/b1 (Hs03302672_pri) and mature miR-29a (ID: 002112) were normalized to endogenous control ACTA (Hs00426835_g1) and U6 snRNA (ID: 001973) respectively. Mouse LOXL2 (Mm00804740_m1) expression was normalized to ACTB (Mm00607939_s1). Samples were run using ABI 7500 Real-Time PCR machine. Relative expressions were analyzed using ΔΔCT method.

Immunofluorescence Imaging

Immunofluorescence Imaging for MYC was performed as described in Supplementary Materials and Methods. Images were obtained using a Leica DM5000B microscope. Quantification of percent MYC nuclear localization was performed using ImageJ software. Data was charted and presented as the average quantification of four replicates for each cell line.

Chromatin Immunoprecipitation (CHIP)

CHIP experiments were carried out as described previously (15,16) with a few modifications as shown in Supplementary Materials and Methods.

Transfection of cultured cell lines

Exponentially growing PCCs were transfected using Dharmafect®1 Reagent (T-2001–01, Dharmacon) and with control (CN-001000–01) or miR-29a mimic (C-300504–07), or the following siRNAs from Dharmacon: siCTRL (D-001810–10-05), siMYC (L-003282–02-0005), siSMAD4 (L-003902–00-0005), siGLI3 (L-011043–00-0005), siMYBL2 (L-010444–00-0005), siLOXL2 (L-008020–01-0005), siCLDN1 (L-017369–00-0005), siHGK (L-003971–00-0002), and siNRAS (L-003919–00-0005), from Qiagen: miRNA inhibitor control (339126) or LNA miR-29a inhibitor (339121), following manufacturer's protocol. Total protein or RNA was isolated 48 hrs post-transfection for western blot or qPCR analyses.

RNA-seq and Bioinformatics

Panc-1 and MIA PaCa-2 cells were transfected with control or miR-29a (n=3/group) following the protocol described above. Total RNA was extracted 48 hrs post-transfection using RNeasy Plus Mini Kit (74134, Qiagen) and the purity was assessed using a Nanodrop 2000. Purified RNA quality was determined by a Bioanalyzer, then used to prepare libraries, and sequenced (pair end read 150 cycles) using an Illumina HiSeq 2000. RNA-seq quality was examined using the FastQC tool. Library obtained from each replicate consisted of 26–36 million short sequence reads that were re-mapped back to the reference genome (hg38) using STAR v2.5 (17), which yielded overall average read map ratios of 93.6% and 90% for Panc-1 and MIA PaCa-2 cell lines. Uniquely mapped sequencing reads were assigned to genes based on Gencode 25 using featureCounts (v1.6.2) (18). After filtering out low expressed genes with read count per million (CPM) <0.5 in greater than two samples, gene expression profiles were normalized using trimmed mean of M values (TMM) method, and

differential expression analysis was performed using edgeR (v3.20.8) (19,20). The differentially expressed genes (DEGs) were determined by cutoff p-value<0.05 after false discovery rate (FDR) adjustment and amplitude of fold change (FC) of gene expression greater than 2 linear FC.

TargetScan (v7.1) (21) was adopted to predict conserved miR-29a target genes. Hypergeometric model was used to calculate the overlap between DEGs and miR-29a predicted targets. Functional enrichment analyses on the DEGs were performed using DAVID (v6.8) database (https://david.ncifcrf.gov/). The miR-29a target gene levels in human PDAC and normal pancreatic tissues were obtained from the human protein atlas (https://www.proteinatlas.org/).

Genetic alterations of the transcription factors with predicted binding sites in pri-miR-29a/b1 promoter in TCGA PDAC datasets were analyzed using the online cBioportal cancer genomics tool (http://www.cbioportal.org/).

Western Blot

Protein lysates were prepared with RIPA Buffer (PI-89900, Thermo Fisher Scientific) and quantified using BCA Protein Assay Kit (23225, Pierce Biotechnology). Equal amounts of total protein were loaded for immunoblot analysis. Immunoblots were probed with antibodies against MYC (5605S, Cell Signaling Technology), SMAD4 (38454S, Cell Signaling Technology), GLI3 (sc-74478, Santa Cruz Biotechnology), MYBL2 (sc-390198, Santa Cruz Biotechnology), LOXL2 (ab96233, Abcam), CLDN1 (4933S, Cell Signaling Technology), HGK (3485, Cell Signaling Technology), NRAS (ab77392, Abcam), E-cadherin (ab40772, Abcam), Vimentin (D21H3, Cell Signaling), LAMB1 (D4Q4Z, Cell Signaling) and GAPDH (MA5–15738, Thermo Fisher Scientific) overnight at 4°C followed by incubation for 1 hr at room temperature with corresponding HRP conjugated goat anti-mouse (31430, Thermo Fisher Scientific) or goat anti-rabbit (31460, Thermo Fisher Scientific) secondary antibodies. Western Blots were then developed using ECL detection kit (34096, Thermo Fisher Scientific) and captured on an Amersham Imager 600 (GE Healthcare). Densitometry analysis was performed using Image J software to quantify each protein band, and were normalized against LAMB1 for nuclear fraction or GAPDH.

Migration Assays

Migration assays with control or transfected Panc-1 and MIA PaCa-2 were performed as described in Supplementary Materials and Methods.

Estimation of Extracellular LOXL2 Secretion

PCCs transfected with control or miR-29a mimic, and siCTRL or siLOXL2 were grown in complete DMEM post-transfection for 24 hrs. 3×10^5 cells were then cultured in serum-free DMEM for 48 hrs. The resulting conditioned media (CM) were collected, and concentrated using Amicon Ultra-0.5 Centrifugal Filter Unit (UFC501096, MilliporeSigma). To quantify the extracellular LOXL2, Enzyme-linked immune sorbent assay (ELISA) was performed with the concentrated CM according to manufacturer's protocol (DY2639–05, R&D Systems).

Collagen Estimation

Sircol Soluble Collagen Assay (Biocolor, Carrickfergus, United Kingdom) and Hydroxyproline Assay were performed as described previously (22) and in the Supplementary Materials and Methods.

Dual Luciferase Reporter Assay

For miR-29a promoter activity, upstream promoter region of miR-29a/b1 containing MYC binding sites was cloned into Luc2 Luciferase Expression vector (E6651, Promega). PCCs were co-transfected with control or siMYC, and MYC binding site Luc2 Luciferase vector using DharmaFECT Duo Transfection Reagent (T-2010–02, Dharmacon). For LOXL2 promoter activity, LOXL2 3'-UTR wild type (3'-UTR WT) and mutant (3'-UTR MUT) luciferase vectors consisting of miR-29a binding site were constructed respectively. The PCCs were co-transfected with control or miR-29a mimic, and 3'-UTR WT, or control or miR-29a mimic, and 3'-UTR MUT. 48 hrs post-transfection, luciferase activity was measured by Dual Glo® Luciferase Assay System (E2920, Promega) following manufacturer's instructions. Firefly luciferase luminescence was normalized to Renilla luciferase activity for each transfected well.

Immunohistochemistry

Immunohistochemistry with human and mouse pancreatic tissue sections was performed as described in Supplementary Materials and Methods.

Statistical Analyses

GraphPad Prism (v5) and Microsoft Excel were used for statistical analyses. All data were expressed as mean ± standard error of the mean (SEM) of three independent experiments. Statistical comparison between two groups was performed using two-tailed Student's t-test, while for multiple comparisons, one-way ANOVA with Bonferroni's correction was used. Chi square tests were performed for correlation analyses between miR-29a and target genes in histopathological samples. $p < 0.05$ was considered as statistically significant and are indicated with asterisks (*$p < 0.05$, **$p<0.01$, ***$p<0.001$).

Results

Pri-miR-29a/b1 expression is lower in PDAC cell lines and inversely correlates with MYC

miR-29 family includes miR-29a, −29b, −29c, encoded by polycistronic hsa-miR-29a/b1 and miR-29c/b2 clusters, located on chr 7q32.3 and 1q32.2 respectively. These clusters are initially transcribed as long pri-miR-29a/b1 and pri-miR-29b2/c (23) and then processed by endonucleases to yield mature miR-29a, −29b and −29c (12,23). Our previous report demonstrated a robust reduction in miR-29a expression in pancreata from a well-characterized Kras-driven PDAC mouse model, KC (LSL-$Kras^{G12D/+}$; *P*dx-1-Cre), PCC lines and human PDAC patients (13). We further demonstrated that among all miR-29 members, miR-29a is most abundantly expressed in human pancreas, pancreatic stellate cells (PSCs), as well as in normal human pancreatic epithelial cell line (HPNE) (13). Therefore, in the current study we primarily focused on primary (pri-) miR-29a/b1 cluster and mature

miR-29a for functional analyses. First, we measured pri-miR-29a/b1 expression levels in four PCC lines (Panc-1, MIA PaCa-2, BxPC-3 and AsPC-1) and two normal human pancreatic ductal epithelial cell lines (HPNE and HPDE). Consistent with our previous observation with mature miR-29a (14), pri-miR-29a/b1 expression was significantly lower in each of the four tested PCC lines as compared to HPNE and HPDE (Fig. 1A).

To understand the potential mechanism of transcriptional repression of miR-29a in pancreatic cancer, we screened several candidate transcription factors (TFs) with predicted binding sites at the miR-29a promoter and are associated with PDAC. This identified five major TFs, namely MYC, SMAD4, YY1, GLI3, and NF-κB. Examining the TCGA pancreatic adenocarcinoma datasets at the cBioPortal, we observed >10% genetic alterations for *MYC* and *SMAD4*, 4% for *GLI3* and little alterations of *NF-κB* and *YY1* in PDAC patients (Fig. 1B). Similar patterns of genetic alterations were observed in PCC data obtained from the Broad Institute Cancer Cell Line Encyclopedia (CCLE) (Supplementary Fig S1–A). In both PDAC patients and PCC lines, *MYC* exhibited the highest copy number alteration (amplification), while *SMAD4* mainly associated with deletion and mutational changes. Interestingly, the miR-29a expression in these TCGA patients and PCC lines inversely correlated with MYC (Fig. 1C, Supplementary Fig S1–B). Because *NF-κB* and *YY1* showed the least genetic alterations in the TCGA patient and CCLE PDAC cell data, and that both the genes are the effectors of the same NF-κB signaling pathway as *GLI3*, we chose to carry out our mechanistic study with MYC, GLI3 and SMAD4 in PCCs, and excluded NF-κB and YY1 from our further analyses.

To determine the association of these three TFs on miR-29a in PDAC, we first performed RNAi mediated knockdown of the TFs in Panc-1 cells (Fig. 1D). Our results indicated a significant (>2 fold) increase in miR-29a expression ($p < 0.05$) only for MYC KD among the tested TFs (Fig. 1E). Further, we observed ~ 2.5 fold increase in the expression of pri-miR-29a/b1 for MYC KD in the Panc-1 cells (Fig. 1F). These results suggested an inverse relationship between MYC and miR-29a and hereafter, we focused on further exploring the regulatory role of MYC on miR-29a in pancreatic cancer.

Inhibition of MYC with small molecule inhibitor enhances miR-29a expression in PCCs

To further validate the repressive regulation of miR-29a by MYC, we treated Panc-1 cells with different doses of a small molecule MYC inhibitor, 10058-F4 (24,25). 10058-F4 resulted in increased expression of miR-29a in a dosage dependent manner, with a significant rise in miR-29a level at 100μM treatment (Fig. 1G). These findings reinforce the inverse regulatory relationship between MYC and miR-29a in PCCs.

PCCs and Normal Pancreatic Epithelial Cells show differential localization of MYC in the nucleus

To find the mechanism of interaction of MYC with miR-29a promoter, we first investigated whether MYC is differentially localized in low and high miR-29a expressing PCCs. Immunofluorescence analysis revealed that in normal pancreatic epithelial cell lines (HPNE and HPDE) expressing higher pri-miR-29a/b1, MYC was minimally localized in the nucleus, while the low pri-miR-29a/b1 expressing PCC lines exhibited strong MYC nuclear

localization (Fig. 2A&B). To validate our immunofluorescence observations, we performed western blot analysis for MYC in the nuclear and cytoplasmic fractions of HPNE cells and PCCs. The MYC expressions were normalized to nuclear protein LAMB1 and cytosolic protein GAPDH for the nuclear and cytosolic fractions respectively, however both the fractions were blotted with LAMB1 and GAPDH to assess the quality of the fractionations. Western blots revealed MYC expression patterns similar to immunofluorescence, corroborating the findings (Fig 2C). In PCC lines, MYC localization was higher in the nucleus and lower in the cytosol, while in HPNE cells, the localization of MYC in the nuclear and cytoplasmic fractions were lower and higher respectively. These findings confirm the negative correlation between MYC and pri-miR-29a/b1 expressions, and indicate that abundance of MYC in the nucleus is likely responsible for miR-29a repression, suggesting a potential interaction between MYC and miR-29a in PCCs.

MYC represses miR-29a by direct promoter binding in PCCs

To gain mechanistic insights into MYC-miR-29a interaction, we next examined if miR-29a/b1 is directly modulated by MYC in PCC lines through promoter activity. MiR-29a/b1 promoter has two conserved MYC binding sites. One of these sites, located at −261 from the transcription start site, contains a canonical E-box binding motif 5’ CACGTG, while the other site located at −1317 consists of a 5’CACATG binding motif (26) (Fig. 2D). To determine the functional significance of these sites, we generated luciferase reporter constructs consisting of a WT miR-29a/b1 promoter which includes the two conserved MYC binding sites. Relative promoter activity was determined by co-transfecting each cell line with promoter luciferase plasmid containing the WT MYC binding sites and siMYC or siCTRL plasmids. In both Panc-1 and MIA PaCa-2 cells, a significantly increased luciferase activity was observed for MYC knockdown, indicating a direct repressive role of MYC in miR-29a expression (Fig. 2E, Supplementary Fig. S1–C). To further validate MYC binding to miR-29a promoter, we performed CHIP assays using the two PCC lines. MYC CHIP was quantified by real-time PCR using two amplicons within the conserved region of miR-29a/b1 along with an amplicon in the *CDKN1A* promoter, which served as a positive control (15). Fold enrichment of the positive control in the MYC CHIP samples compared to CHIP samples with IgG antibody was set as the threshold (>12 folds) for MYC binding. In both PCC lines, MYC CHIP signals crossed the fold enrichment threshold, confirming the association of MYC with the repressed miR-29a/b1 promoter (Fig. 2F, Supplementary Fig. S1–D).Together, these results show that in PCCs, MYC directly binds to the promoter elements of miR-29a/b1 and represses miR-29a transcription.

RNA-seq identifies differentially expressed miR-29a targets

We next sought to identify global miR-29a effectors and delineate the downstream signaling mechanisms of miR-29a in PDAC. High-throughput RNA-seq with Panc-1 and MIA PaCa-2 cells overexpressing miR-29a, along with those transfected with mimic control, generated a global miR-29a targetome. For analyzing the RNA-seq data and identifying the critical miR-29a targets, we employed a pipeline depicted in Figure 3A. RNA-seq dataset for Panc-1 identified 6687 downregulated and 6311 upregulated genes while MIA PaCa-2 dataset revealed 7457 and 7633 down- and upregulated transcripts respectively (Fig. 3B, Supplementary Fig. S2–A). The differentially expressed genes (DEGs) for Panc-1 and MIA

PaCa-2 datasets exhibited high degree of correlation (Pearson's Correlation Coefficient =0.69) (Fig. 3C). Thereafter, we applied stringent filters and considered only those DEGs which met the following criteria: logFC >± 1, FDR<0.05 and p<0.05. This identified 278 and 369 genes in Panc-1, and 556 and 440 genes in MIA PaCa-2 datasets that were down- and up- regulated respectively (Fig. 3D, Supplementary Fig. S2–B). Next, we used TargetScan database (27) to identify predicted putative miR-29a targets among the DEGs in the two datasets. In both datasets, majority of the miR-29a targets were downregulated (Fig. 3D, Supplementary Fig. S2–B). In Panc-1 dataset, of the downregulated genes, 108 genes were miR-29a targets, while 5 of the upregulated genes were miR-29a targets (Fig. 3D). Again, in MIA PaCa-2 dataset, 80 of all downregulated genes and 15 of all upregulated genes were predicted miR-29a targets (Fig. 3D). Comparison of the DEGs among the Panc-1 and MIA PaCa-2 datasets revealed 43 downregulated, and 4 upregulated miR-29a target genes that overlapped in the two datasets (Fig. 3D, Supplementary Fig. S2–B, Supplementary Table S2). A subset of top 30 overlapping DEGs, with the highest average fold changes in Panc-1 and MIA Paca-2 cell lines, were subjected to qPCR, and all of the 30 genes well-matched in magnitude and direction of expression, validating the RNA-seq data (Supplementary Table S3). Because majority of the miR-29a targets were downregulated in both the datasets, we focused on the resultant overlapping downregulated targets for further analyses. Consistent with our data, increasing evidence demonstrated the significance of miR-29a in variety of cancers, and majority of these studies have shown miR-29a to function as a tumor suppressor by downregulating oncogenes (12,14,28,29).

Target Enrichment, Gene Ontology (GO) and The Cancer Genome Atlas (TCGA) data analyses identify top miR-29a targets and their functional attributes in PDAC

To determine the biological function and signaling pathways associated with the miR-29a targets, pathway enrichment analysis was performed for the genes by inputting their Entrenz IDs into the functional annotation tool DAVID, and the genes were grouped one or more of the following four GO categories: ECM Related, Migration/Invasion, Cancer/Growth/Proliferation, and Metabolism, based on relevant GO terms (30). Pathway analysis of the 20 most differentially expressed overlapping upregulated genes identified 11 genes belonging to one of the four GO categories, but none of these genes were miR-29a targets. Of the top 20 downregulated genes, 13 belonged to the GO categories, among which 10 genes were miR-29a targets (Supplementary Fig. S2–C). Overall, high enrichment scores and significant association of a vast majority of the miR-29a targets with individual GO terms was observed in each category (Fig. 3E and F). These findings are in agreement with the mechanisms of PDAC progression, which is characterized by desmoplasia, epithelial mesenchymal transition (EMT), metastasis, altered metabolism and drug resistance (4,31). To determine the most clinically relevant miR-29a targets and their prognostic impacts, we performed survival analysis for the 43 downregulated genes using publicly available TCGA patient data. This pipeline identified the seven miR-29a targets from the RNA-seq datasets-MYBL2/b-myb, LOXL2, CLDN1, MAP4K4/HGK, NRAS, FNDC5 and TUBD1 (Table 1) with highest fold changes in mRNA expressions in RNA-seq and logrank p <0.05 for Kaplan-Meier survival correlation analyses from TCGA data. Interestingly, Kaplan-Meier curve and log rank test analyses in pancreatic adenocarcinoma patients showed that lower expression of five of these genes, except FNDC5 and TUBD1, correlated with higher overall

survival of the patients (Fig. 4A). Consistently, the univariate Cox Proportional Hazard Regression model indicated a higher hazard risk in the patients for high expression of the five genes while a lower risk with higher expression of FNDC5 and TUBD1 (Table 1). Our previous reports and other studies in diverse tumor types document miR-29a to function as a tumor suppressor. Thus, hereafter we focused on the five targets of MYBL2, LOXL2, CLDN1, HGK and NRAS, where lower gene expression associated with better prognosis.

Restoration of miR-29a in PDAC cell lines downregulates target genes

To evaluate the effect of miR-29a on these five candidate targets, we performed western blot analysis in Panc-1 and MIA PaCa-2 cell lines transfected with control or miR-29a mimics at three different concentrations (5nM, 10nM and 20nM). For each 10nM and 20nM miR-29a dosage, expressions of all the five target proteins were significantly reduced in the two cell lines (Fig. 4B, Supplementary Fig. S3–A). However, for the 5nM dosage, the reduction in protein levels reached a significant threshold for the four genes except NRAS (Fig. 4B, Supplementary Fig. S3–A). This finding confirms a miR-29a mediated translational suppression mechanism in the five tested miR-29a targets.

Silencing the candidate targets reduces migration and EMT phenotypes in PDAC cells

GO analysis indicated the five identified targets to associate with cell migration mechanisms. Thus, to determine the effect of these candidates in PCC migration, we silenced the expression of the genes in Panc-1 and MIA PaCa-2 cells and seeded the cells for transwell assays. Knock-down of all the five targets significantly inhibited the migratory potential of the cells in MIA PaCa-2 cell line, with approximately 50% reduction in migration ability for LOXL2 (Supplementary Fig. S3–B). Significant reduction in migratory ability was observed in Panc-1 cells for four of the targets, except CLDN1 (Fig. 4C). Interestingly, in both Panc-1 and MIA PaCa-2 cell lines, among all five targets, silencing LOXL2 resulted in the highest inhibition of the migration of the cancer cells by around 50%, which mimics the migratory potential of miR-29a overexpressing cancer cells (Fig. 4C, Supplementary Fig. S3–B). Therefore, our data indicate that restoration of miR-29a or depletion of its downstream targets markedly impedes the migratory potential of PCCs.

Previously, we demonstrated that overexpressing miR-29a diminishes EMT phenotype in Panc-1 cell line (14). Here, we examined the effect of silencing the five miR-29a targets on EMT in the cell line (Fig. 4D). Western blot analysis showed that silencing each of the five targets resulted in increased expression of epithelial marker, E-cadherin, and decreased mesenchymal marker vimentin, with the most robust effects for siLOXL2 and siMYBL2. Together, these results suggest an association of miR-29a and its key targets with PDAC metastasis.

LOXL2 is a direct miR-29a target in PDAC cells

We next narrowed our focus on to LOXL2 as a primary candidate to perform additional functional analyses to elucidate miR-29a-LOXL2 axis in PDAC regulation. Firstly, LOXL2 exhibited one of the highest fold changes among the downregulated targets in our primary candidate list from RNA-seq, and downregulation of the gene was most significantly correlated with survival in TCGA PDAC patients. Additionally, miR-29a gain-of-function

resulted in a robust depletion of LOXL2 protein expression, and loss of LOXL2 maximally impeded PCC migration and EMT. Given the unique tumor-stromal crosstalk associated with PDAC histopathology, *LOXL2* appears to be the most relevant gene to study, being the only target that exhibits both intracellular and secreted functions in inducing EMT/metastatic phenotypes and regulating stromal remodeling via collagen crosslinking respectively (32,33).

To determine if LOXL2 is a direct miR-29a target in PCC lines, we identified the two putative miR-29a binding sites at the 3'-UTR of LOXL2 (positions 555–561 and 757–763) using TargetScan database. We then designed luciferase reporter assay with a vector encoding either WT LOXL2 miR-29a 3'-UTR binding site, or a sequence consisting of alternating point mutations within the miR-29a target binding region (Fig. 5A). Consistent with the predicted downregulatory role of miR-29a on LOXL2, we observed significantly reduced (~ 50%) luciferase activity for the Panc-1 and MIA PaCa-2 cells co-transfected with WT 3'-UTR carrying vector and miR-29a as compared to the non-specific control mimics, while co-transfection with the mutated 3'-UTR vector resulted in enhanced luminescence intensity abolishing the inhibitory effects of miR-29a (Fig. 5B, Supplementary Fig. S4–A). These data confirm that miR-29a directly binds to the 3'-UTR region of LOXL2 and negatively regulates the expression of the gene in PCC lines. Expectedly, silencing LOXL2 had no effect on miR-29a expression in the two PCC cell lines (Supplementary Fig. S4–B). Next, to assess the MYC-miR-29a axis in regulation of LOXL2 expression, we first silenced MYC, which resulted in reduction of LOXL2 in Panc-1 and MIA PaCa-2 cell lines (Fig. 5C, Supplementary Fig. S4–C). Thereafter, we inhibited (i) miR-29a alone, or (ii) miR-29a and MYC simultaneously, both of which resulted in increased LOXL2 expressions (Fig. 5D). These observations suggest that LOXL2 expression is directly dependant on miR-29a in PCCs in MYC-silenced cells.

Gain of miR-29a function diminishes extracellular LOXL2 in PCCs

Because LOXL2 is a secreted protein and tumor-derived LOXL2 is known to influence tumor microenvironment, we next sought to study if miR-29a has an effect on extracellular LOXL2 function in PDAC. To this end, we analyzed the levels of secreted LOXL2 in CM obtained from Panc-1 and MIA PaCa-2 cells transfected with control or miR-29a mimics, and siCTRL or siLOXL2. Our results showed that in Panc-1 and MIA PaCa-2 cell lines, gain of miR-29a function resulted in 71% and 62% reduction in secreted LOXL2 levels respectively in the CM (Fig. 5E, Supplementary Fig. S4–D). To further validate whether ectopic miR-29a expression affected extracellular collagen crosslinking function of LOXL2, we estimated the newly crosslinked pepsin-soluble and heavily crosslinked insoluble collagen levels using Sircol and hydroxyproline assays respectively in the two PCC lines transfected with control or miR-29a mimics, and siCTRL or siLOXL2. Consistently, overexpressing miR-29a markedly depleted soluble and insoluble crosslinked collagen contents in the PCCs, similar to the effect observed for silencing LOXL2 (Fig. 5F&G, Supplementary Fig. S4–E&F). These results validate the regulatory role of miR-29a in extracellular collagen-crosslinking LOXL2 activity.

Enhanced LOXL2 levels with reduced miR-29a expression observed in PanIN lesions/ PDAC in GEMM and clinical patient specimens

To assess the association between miR-29a and LOXL2 expression in PDAC *in vivo* and substantiate its clinical relevance, we first determined LOXL2 expression levels by immunohistochemistry analysis in pancreatic tissue samples from 4–6 months old mice belonging to a well characterized PDAC mouse model, KPC, that expresses the most common human oncogenic *Kras* (cancer-driver) and *p53* (tumor-suppressor) mutations ($Kras^{LSL.G12D/+}$; $p53^{R172H/+}$; Pdx1-Cre), as well as in PDAC patient biopsies consisting of 35–80% tumor stroma. In both KPC mice and clinical specimens, LOXL2 was highly expressed in pancreata with advanced PanIN or PDAC lesions, with little or no expression in normal regions or healthy tissues (Fig. 6A). Next, we evaluated the expression levels of LOXL2 and miR-29a in the pancreatic tissue samples from KPC mice via qPCR and compared that with age matched C57BL/6 control mice. In agreement with our *in vitro* observations, miR-29a expression in the KPC pancreatic tissue samples was significantly lower than the control C57BL/6 specimens with concomitant higher LOXL2 expression in KPC compared to C57BL/6 mouse tissues (Fig. 6B), confirming a negative correlation between miR-29a and LOXL2 *in vivo*. In our previous report, we demonstrated a significant reduction of miR-29a in PDAC patient tumors as compared to normal patient control pancreata (13). In TCGA PDAC patient data (n=178), although a small correlation was observed between miR-29a and LOXL2 by Pearson's correlation test ($R = -0.21$), the inverse association was statistically significant ($p = 3.9e^{-03}$), indicating a potential effect of the relationship in the context of PDAC patient prognosis (Fig. 6C). Together, these findings suggest that upregulation of LOXL2 is accompanied by concomitant suppression of miR-29a in PDAC *in vivo*, contributing to the disease progression.

Discussion

In the current study, we aimed to gain mechanistic insights into the upstream regulation of miR-29a, identify its global downstream effectors and discern their roles in PDAC pathogenesis. Here, we elucidate a novel miR-29a-mediated regulatory axis in PDAC pathogenesis. We have previously shown that in PCCs, pri-miR-29a/b1 and mature miR-29a expressions are commonly repressed compared to normal pancreatic epithelial cells (14) (Fig. 1A). Utilizing orthogonal loss-of-function approaches through siRNA mediated knockdown and small molecule inhibition, here we observed that miR-29a is repressed by MYC in PCCs. Because prior studies had indicated direct repressional regulation of several microRNAs including miR-29a by MYC in varied types of cells (15,26,34), we performed CHIP and luciferase assays to understand the regulation in PDAC. Our CHIP data demonstrated a direct binding of MYC at the miR-29a/b1 promoter binding site- a site where MYC was previously shown to repress miR-29a expression by recruiting EZH2 and causing H3K27 methylation mediated chromatin condensation (26,34). We further confirm a MYC-mediated repression of miR-29a at this binding site by luciferase assay. Thus, observations reported in the current study, in conjunction with prior evidence, suggest a direct MYC-mediated miR29a repression in pancreatic cancer.

MYC is one of the central oncogenic TFs that is upregulated in approximately 40% of PDAC cases (35). *MYC* transcription is shown to be repressed by TGF-β/SMAD signaling, when TGF- β acts as a tumor-suppressor (36). Numerous studies have confirmed the context specific, paradoxical role of TGF-β in cancer (37–39). At early stages of tumorigenesis, TGF-β exhibits tumor-suppressive activities, while it "switches" to a pro-tumorigenic gene at a later stage in response to changes in the tumor microenvironment and mutations in *Kras*, which mediate inactivating mutations in tumor-suppressor genes *CDKN2A*, *TP53* and *SMAD4* (38–40). Notably, transition of PanIN to PDAC is characterized by the same activated *Kras* mutations (41). On the other hand, MYC is also a crucial downstream effector of Kras in the pancreatic cancer (42). Our previous findings demonstrate a pro-tumorigenic effect of TGF-β in pancreatic cancer, where we show that TGF-β1/SMAD4 signaling downregulates miR-29a expression in activated pancreatic stellate cells (PSCs) (13). In the same study we observed loss of miR-29a in Kras induced PDAC mice (13). Given that MYC is a downstream effector of both TGF-β and Kras signaling pathways- the pathways that also regulate miR-29a expression in PCCs, it is possible that the repression of miR-29a by MYC promoter binding is regulated by the Kras-TGF-β axis, or either by Kras or TGF-β signaling alone. However, it will be essential to design future studies to validate this supposition and further explore the upstream MYC-miR-29a regulatory axis in PDAC based on the current perspectives.

Our current RNA-seq offers one of the most comprehensive data on miR-29a regulated transcriptome in pancreatic cancer. We identified that the expression of 43 downstream miR-29a target genes, involved in ECM remodeling, cell migration, cellular growth and proliferation and/or metabolism, are reduced in PCC cells with restoration of miR-29a function. We found that in PCCs, miR-29a downregulates the expression of five prominent oncogenic targets (*MYBL2*, *LOXL2*, *CLDN1*, *HGK* and *NRAS*) both at transcriptional and translational levels. These five genes are particularly relevant in the context of PDAC because of their functional roles in mediating either or both ECM remodeling and cell migration/ metastasis- the classic mechanisms of PDAC progression, via diverse signaling pathways. For example, *NRAS* and *HGK* promote cell migration and proliferation via PI3K/Akt and JNK/ p38 pathways respectively (43,44). While *CLDN1* is a tight junction protein known to promote cell migration/ invasion and EMT via Wnt/ β-catenin pathway (45), *MYBL2* and *LOXL2* promote both cancer cell proliferation and stromal desmoplasia via pathways such as Akt, NF-κβ, and Src/FAK (46–48). Here we show for the first time a miR-29a mediated regulatory axis of these genes in PDAC. Our findings suggest that loss of miR-29a in PCCs escalates tumor progression by de-repression of these pro-tumorigenic targets, perturbing the homeostasis of the cells. To assess the clinical relevance of the identified miR-29a-target regulatory axes, we compared the mRNA expressions of the genes with miR-29a from publicly available pancreatic adenocarcinoma patient datasets. The analysis revealed a negative correlation between the expressions of *LOXL2*, *CLDN1*, *HGK* and *NRAS* with miR-29a, largely supporting our data (Fig. 6C, Supplementary Fig. S5). Lack of a negative correlation between *MYBL2* and miR-29a expressions perhaps reflects the heterogeneity in the biopsy specimens or its combination with other genetic factors associated with PDAC. Nonetheless, our findings advocate that restored expression of miR-29a in PDAC could offer a therapeutic advantage- the molecule being a single key

regulatory node to modulate multiple oncogenic targets associated with essential intra- and extracellular signaling pathways of tumor-stromal crosstalk, which are pivotal for the disease progression. Although the current work centers on further unraveling of the mechanisms of miR-29a-LOXL2 axis, future studies should be designed to functionally characterize each of the other four target genes of *MYBL2*, *CLDN1*, *HGK* and *NRAS* and their miR-29a mediated regulatory pathways in PDAC tumorigenesis.

Our data in this study show that in PCCs, miR-29a perturbs both intracellular and secreted LOXL2 function by repressing LOXL2 transcription via 3'-UTR binding. We observed increased levels of LOXL2 in both KPC mice and patient biopsy specimens, with inverse relationship with miR-29a (Fig. 6). Our *in vitro* study further indicates that loss of LOXL2 in PCCs reduces the migration potential and EMT, which is consistent with other reports that demonstrate an intracellular, EMT promoting, LOXL2 function. Particularly, studies have shown that LOXL2 promotes EMT by direct downregulation of E-cadherin via interaction with Snail, a key TF in pancreatic cancer (49). Interestingly, we previously observed that overexpression of miR-29a results in an increase in E-cadherin in PCCs inducing mesenchymal-epithelial transition (MET) (14). However, E-cadherin is not a predicted miR-29a target (TargetScan), suggesting miR-29a to be an indirect player in E-cadherin regulation. This aligns with our current observations, and given our findings, it is reasonable to speculate that LOXL2 is likely the intermediate that bridges the gap between miR-29a and E-cadherin in regulation of EMT. Thus, our data support that in PCCs, repression of miR-29a de-represses LOXL2, which possibly promotes LOXL2-Snail interaction resulting in the downregulation of E-cadherin to escalate EMT phenotypes.

In our previous report, we have shown an anti-fibrotic function of miR-29a in pancreatic cancer tumor microenvironment, where miR-29a was found to inhibit major stromal protein expression and excessive stromal deposition by activated PSC (13). Here in this study, we evidence that restored expression of miR-29a in PCCs blocks LOXL2 secretion by the cancer cells potentially impeding the extracellular collagen crosslinking function of the protein. These observations are of great significance in the context of PDAC, where activated stroma is associated with poor patient prognosis and clinical outcome, and promotes aggressive, metastatic progression of the disease (4,50). Thus, it is apparent from our findings that the paracrine effect of miR-29a could encumber the transformation of quiescent PSCs to activated CAFs in the PDAC tumor microenvironment hindering metastasis-promoting stromal remodeling in the disease to facilitate efficient drug delivery to the tumor core.

Taken together, the current report provides novel insights into the regulatory mechanisms of miR-29a in inducing tumor-suppressive networks in PDAC, and advocates the importance of this molecule for therapeutic intervention. While our *in vitro*, *in vivo* and clinical observations elucidate the regulation and effects of the loss of miR-29a, and a MYC-miR-29a-LOXL2 regulatory axis in PDAC, future studies using miR-29a knock-out mouse models will aid in further characterization of the regulatory role of the molecule in a physiological context, allowing to assess the prognostic and therapeutic appositeness of the molecule in targeting the disease.

Supplementary Material

Refer to Web version on PubMed Central for supplementary material.

Acknowledgements

We thank the IU Pathology and the IU Cancer Center Tissue Bank for histological stains and human tissue samples. We thank Mr. Max H. Jacobsen and Dr. George E. Sandusky for their assistance and guidance in acquiring and interpreting the histopathological data. This work is supported by the Research Scholar Grant, RSG-18-105-01-RMC from the American Cancer Society and by the NIH/NCRR Grant UL1TR001108 from the Indiana CTSI to JK. JJK was supported by NCI Grant 1 F31 CA213731-01A1.

References

1. Siegel RL, Miller KD, Jemal A. Cancer Statistics, 2017. CA Cancer J Clin 2017;67(1):7–30 doi 10.3322/caac.21387. [PubMed: 28055103]
2. Hidalgo M, Cascinu S, Kleeff J, Labianca R, Lohr JM, Neoptolemos J, et al. Addressing the challenges of pancreatic cancer: future directions for improving outcomes. Pancreatology 2015;15(1):8–18 doi 10.1016/j.pan.2014.10.001. [PubMed: 25547205]
3. Rahib L, Smith BD, Aizenberg R, Rosenzweig AB, Fleshman JM, Matrisian LM. Projecting cancer incidence and deaths to 2030: the unexpected burden of thyroid, liver, and pancreas cancers in the United States. Cancer Res 2014;74(11):2913–21 doi 10.1158/0008-5472.CAN-14-0155. [PubMed: 24840647]
4. Kota J, Hancock J, Kwon J, Korc M. Pancreatic cancer: Stroma and its current and emerging targeted therapies. Cancer Lett 2017;391:38–49 doi 10.1016/j.canlet.2016.12.035. [PubMed: 28093284]
5. Ren B, Cui M, Yang G, Wang H, Feng M, You L, et al. Tumor microenvironment participates in metastasis of pancreatic cancer. Mol Cancer 2018;17(1):108 doi 10.1186/s12943-018-0858-1. [PubMed: 30060755]
6. Kanda M, Matthaei H, Wu J, Hong SM, Yu J, Borges M, et al. Presence of somatic mutations in most early-stage pancreatic intraepithelial neoplasia. Gastroenterology 2012;142(4):730–3 e9 doi 10.1053/j.gastro.2011.12.042. [PubMed: 22226782]
7. Hezel AF, Kimmelman AC, Stanger BZ, Bardeesy N, Depinho RA. Genetics and biology of pancreatic ductal adenocarcinoma. Genes Dev 2006;20(10):1218–49 doi 10.1101/gad.1415606. [PubMed: 16702400]
8. Maitra A, Adsay NV, Argani P, Iacobuzio-Donahue C, De Marzo A, Cameron JL, et al. Multicomponent analysis of the pancreatic adenocarcinoma progression model using a pancreatic intraepithelial neoplasia tissue microarray. Mod Pathol 2003;16(9):902–12 doi 10.1097/01.MP.0000086072.56290.FB. [PubMed: 13679454]
9. Ledford H Cancer: The Ras renaissance. Nature 2015;520(7547):278–80 doi 10.1038/520278a. [PubMed: 25877186]
10. Cox AD, Fesik SW, Kimmelman AC, Luo J, Der CJ. Drugging the undruggable RAS: Mission possible? Nat Rev Drug Discov 2014;13(11):828–51 doi 10.1038/nrd4389. [PubMed: 25323927]
11. Collins MA, Pasca di Magliano M. Kras as a key oncogene and therapeutic target in pancreatic cancer. Front Physiol 2013;4:407 doi 10.3389/fphys.2013.00407. [PubMed: 24478710]
12. Kwon JJ, Factora TD, Dey S, Kota J. A Systematic Review of miR-29 in Cancer. Mol Ther Oncolytics 2019;12:173–94 doi 10.1016/j.omto.2018.12.011. [PubMed: 30788428]
13. Kwon JJ, Nabinger SC, Vega Z, Sahu SS, Alluri RK, Abdul-Sater Z, et al. Pathophysiological role of microRNA-29 in pancreatic cancer stroma. Sci Rep 2015;5:11450 doi 10.1038/srep11450. [PubMed: 26095125]
14. Kwon JJ, Willy JA, Quirin KA, Wek RC, Korc M, Yin XM, et al. Novel role of miR-29a in pancreatic cancer autophagy and its therapeutic potential. Oncotarget 2016;7(44):71635–50 doi 10.18632/oncotarget.11928. [PubMed: 27626694]

15. Chang TC, Yu D, Lee YS, Wentzel EA, Arking DE, West KM, et al. Widespread microRNA repression by Myc contributes to tumorigenesis. Nat Genet 2008;40(1):43–50 doi 10.1038/ng.2007.30. [PubMed: 18066065]

16. Barrilleaux BL, Cotterman R, Knoepfler PS. Chromatin immunoprecipitation assays for Myc and N-Myc. Methods Mol Biol 2013;1012:117–33 doi 10.1007/978-1-62703-429-6_9. [PubMed: 24006062]

17. Dobin A, Davis CA, Schlesinger F, Drenkow J, Zaleski C, Jha S, et al. STAR: ultrafast universal RNA-seq aligner. Bioinformatics 2013;29(1):15–21 doi 10.1093/bioinformatics/bts635. [PubMed: 23104886]

18. Liao Y, Smyth GK, Shi W. featureCounts: an efficient general purpose program for assigning sequence reads to genomic features. Bioinformatics 2014;30(7):923–30 doi 10.1093/bioinformatics/btt656. [PubMed: 24227677]

19. Robinson MD, McCarthy DJ, Smyth GK. edgeR: a Bioconductor package for differential expression analysis of digital gene expression data. Bioinformatics 2010;26(1):139–40 doi 10.1093/bioinformatics/btp616. [PubMed: 19910308]

20. McCarthy DJ, Chen Y, Smyth GK. Differential expression analysis of multifactor RNA-Seq experiments with respect to biological variation. Nucleic Acids Res 2012;40(10):4288–97 doi 10.1093/nar/gks042. [PubMed: 22287627]

21. Agarwal V, Bell GW, Nam JW, Bartel DP. Predicting effective microRNA target sites in mammalian mRNAs. Elife 2015;4 doi 10.7554/eLife.05005.

22. Rosell-Garcia T, Rodriguez-Pascual F. Enhancement of collagen deposition and crosslinking by coupling lysyl oxidase with bone morphogenetic protein-1 and its application in tissue engineering. Sci Rep 2018;8(1):10780 doi 10.1038/s41598-018-29236-6. [PubMed: 30018337]

23. Lee Y, Ahn C, Han J, Choi H, Kim J, Yim J, et al. The nuclear RNase III Drosha initiates microRNA processing. Nature 2003;425(6956):415–9 doi 10.1038/nature01957. [PubMed: 14508493]

24. Guo J, Parise RA, Joseph E, Egorin MJ, Lazo JS, Prochownik EV, et al. Efficacy, pharmacokinetics, tisssue distribution, and metabolism of the Myc-Max disruptor, 10058-F4 [Z,E]-5-[4-ethylbenzylidine]-2-thioxothiazolidin-4-one, in mice. Cancer Chemother Pharmacol 2009;63(4):615–25 doi 10.1007/s00280-008-0774-y. [PubMed: 18509642]

25. Huang MJ, Cheng YC, Liu CR, Lin S, Liu HE. A small-molecule c-Myc inhibitor, 10058-F4, induces cell-cycle arrest, apoptosis, and myeloid differentiation of human acute myeloid leukemia. Exp Hematol 2006;34(11):1480–9 doi 10.1016/j.exphem.2006.06.019. [PubMed: 17046567]

26. Mott JL, Kurita S, Cazanave SC, Bronk SF, Werneburg NW, Fernandez-Zapico ME. Transcriptional suppression of mir-29b-1/mir-29a promoter by c-Myc, hedgehog, and NF-kappaB. J Cell Biochem 2010;110(5):1155–64 doi 10.1002/jcb.22630. [PubMed: 20564213]

27. Lewis BP, Shih IH, Jones-Rhoades MW, Bartel DP, Burge CB. Prediction of mammalian microRNA targets. Cell 2003;115(7):787–98. [PubMed: 14697198]

28. Mazzoccoli L, Robaina MC, Apa AG, Bonamino M, Pinto LW, Queiroga E, et al. MiR-29 silencing modulates the expression of target genes related to proliferation, apoptosis and methylation in Burkitt lymphoma cells. Journal of cancer research and clinical oncology 2018;144(3):483–97 doi 10.1007/s00432-017-2575-3. [PubMed: 29318382]

29. Qu H, Zhu M, Tao Y, Zhao Y. Suppression of peripheral myelin protein 22 (PMP22) expression by miR29 inhibits the progression of lung cancer. Neoplasma 2015;62(6):881–6 doi 10.4149/neo_2015_107. [PubMed: 26458320]

30. Ashburner M, Ball CA, Blake JA, Botstein D, Butler H, Cherry JM, et al. Gene ontology: tool for the unification of biology. The Gene Ontology Consortium. Nat Genet 2000;25(1):25–9 doi 10.1038/75556. [PubMed: 10802651]

31. Neesse A, Algul H, Tuveson DA, Gress TM. Stromal biology and therapy in pancreatic cancer: a changing paradigm. Gut 2015;64(9):1476–84 doi 10.1136/gutjnl-2015-309304. [PubMed: 25994217]

32. Okada K, Moon HJ, Finney J, Meier A, Mure M. Extracellular Processing of Lysyl Oxidase-like 2 and Its Effect on Amine Oxidase Activity. Biochemistry 2018;57(51):6973–83 doi 10.1021/acs.biochem.8b01008. [PubMed: 30499665]

33. Cui X, Wang G, Shen W, Huang Z, He H, Cui L. Lysyl oxidase-like 2 is highly expressed in colorectal cancer cells and promotes the development of colorectal cancer. Oncol Rep 2018;40(2): 932–42 doi 10.3892/or.2018.6452. [PubMed: 29845296]
34. Zhang X, Zhao X, Fiskus W, Lin J, Lwin T, Rao R, et al. Coordinated silencing of MYC-mediated miR-29 by HDAC3 and EZH2 as a therapeutic target of histone modification in aggressive B-Cell lymphomas. Cancer Cell 2012;22(4):506–23 doi 10.1016/j.ccr.2012.09.003. [PubMed: 23079660]
35. Hessmann E, Schneider G, Ellenrieder V, Siveke JT. MYC in pancreatic cancer: novel mechanistic insights and their translation into therapeutic strategies. Oncogene 2016;35(13):1609–18 doi 10.1038/onc.2015.216. [PubMed: 26119937]
36. Yagi K, Furuhashi M, Aoki H, Goto D, Kuwano H, Sugamura K, et al. c-myc is a downstream target of the Smad pathway. J Biol Chem 2002;277(1):854–61 doi 10.1074/jbc.M104170200. [PubMed: 11689553]
37. Inman GJ. Switching TGFbeta from a tumor suppressor to a tumor promoter. Curr Opin Genet Dev 2011;21(1):93–9 doi 10.1016/j.gde.2010.12.004. [PubMed: 21251810]
38. Bierie B, Moses HL. Tumour microenvironment: TGFbeta: the molecular Jekyll and Hyde of cancer. Nature reviews Cancer 2006;6(7):506–20 doi 10.1038/nrc1926. [PubMed: 16794634]
39. Lebrun JJ. The Dual Role of TGFbeta in Human Cancer: From Tumor Suppression to Cancer Metastasis. ISRN Mol Biol 2012;2012:381428 doi 10.5402/2012/381428. [PubMed: 27340590]
40. Grusch M, Petz M, Metzner T, Ozturk D, Schneller D, Mikulits W. The crosstalk of RAS with the TGF-beta family during carcinoma progression and its implications for targeted cancer therapy. Curr Cancer Drug Targets 2010;10(8):849–57. [PubMed: 20718708]
41. Dunne RF, Hezel AF. Genetics and Biology of Pancreatic Ductal Adenocarcinoma. Hematol Oncol Clin North Am 2015;29(4):595–608 doi 10.1016/j.hoc.2015.04.003. [PubMed: 26226899]
42. Walz S, Lorenzin F, Morton J, Wiese KE, von Eyss B, Herold S, et al. Activation and repression by oncogenic MYC shape tumour-specific gene expression profiles. Nature 2014;511(7510):483–7 doi 10.1038/nature13473. [PubMed: 25043018]
43. Li Y, Shan Z, Liu C, Yang D, Wu J, Men C, et al. MicroRNA-294 Promotes Cellular Proliferation and Motility through the PI3K/AKT and JAK/STAT Pathways by Upregulation of NRAS in Bladder Cancer. Biochemistry (Mosc) 2017;82(4):474–82 doi 10.1134/S0006297917040095. [PubMed: 28371605]
44. Mc Gee MM, Campiani G, Ramunno A, Nacci V, Lawler M, Williams DC, et al. Activation of the c-Jun N-terminal kinase (JNK) signaling pathway is essential during PBOX-6-induced apoptosis in chronic myelogenous leukemia (CML) cells. J Biol Chem 2002;277(21):18383–9 doi 10.1074/jbc.M112058200. [PubMed: 11856743]
45. Wu X, Xiao J, Zhao C, Zhao C, Han Z, Wang F, et al. Claudin1 promotes the proliferation, invasion and migration of nasopharyngeal carcinoma cells by upregulating the expression and nuclear entry of beta-catenin. Exp Ther Med 2018;16(4):3445–51 doi 10.3892/etm.2018.6619. [PubMed: 30233694]
46. Park JS, Lee JH, Lee YS, Kim JK, Dong SM, Yoon DS. Emerging role of LOXL2 in the promotion of pancreas cancer metastasis. Oncotarget 2016;7(27):42539–52 doi 10.18632/oncotarget.9918. [PubMed: 27285767]
47. Zhang X, Lv QL, Huang YT, Zhang LH, Zhou HH. Akt/FoxM1 signaling pathway-mediated upregulation of MYBL2 promotes progression of human glioma. Journal of experimental & clinical cancer research : CR 2017;36(1):105 doi 10.1186/s13046-017-0573-6. [PubMed: 28784180]
48. Shao M, Ren Z, Zhang R. MYBL2 protects against H9c2 injury induced by hypoxia via AKT and NFkappaB pathways. Mol Med Rep 2018;17(3):4832–8 doi 10.3892/mmr.2018.8387. [PubMed: 29328450]
49. Peinado H, Del Carmen Iglesias-de la Cruz M, Olmeda D, Csiszar K, Fong KS, Vega S, et al. A molecular role for lysyl oxidase-like 2 enzyme in snail regulation and tumor progression. EMBO J 2005;24(19):3446–58 doi 10.1038/sj.emboj.7600781. [PubMed: 16096638]
50. Erkan M, Michalski CW, Rieder S, Reiser-Erkan C, Abiatari I, Kolb A, et al. The activated stroma index is a novel and independent prognostic marker in pancreatic ductal adenocarcinoma. Clin Gastroenterol Hepatol 2008;6(10):1155–61 doi 10.1016/j.cgh.2008.05.006. [PubMed: 18639493]

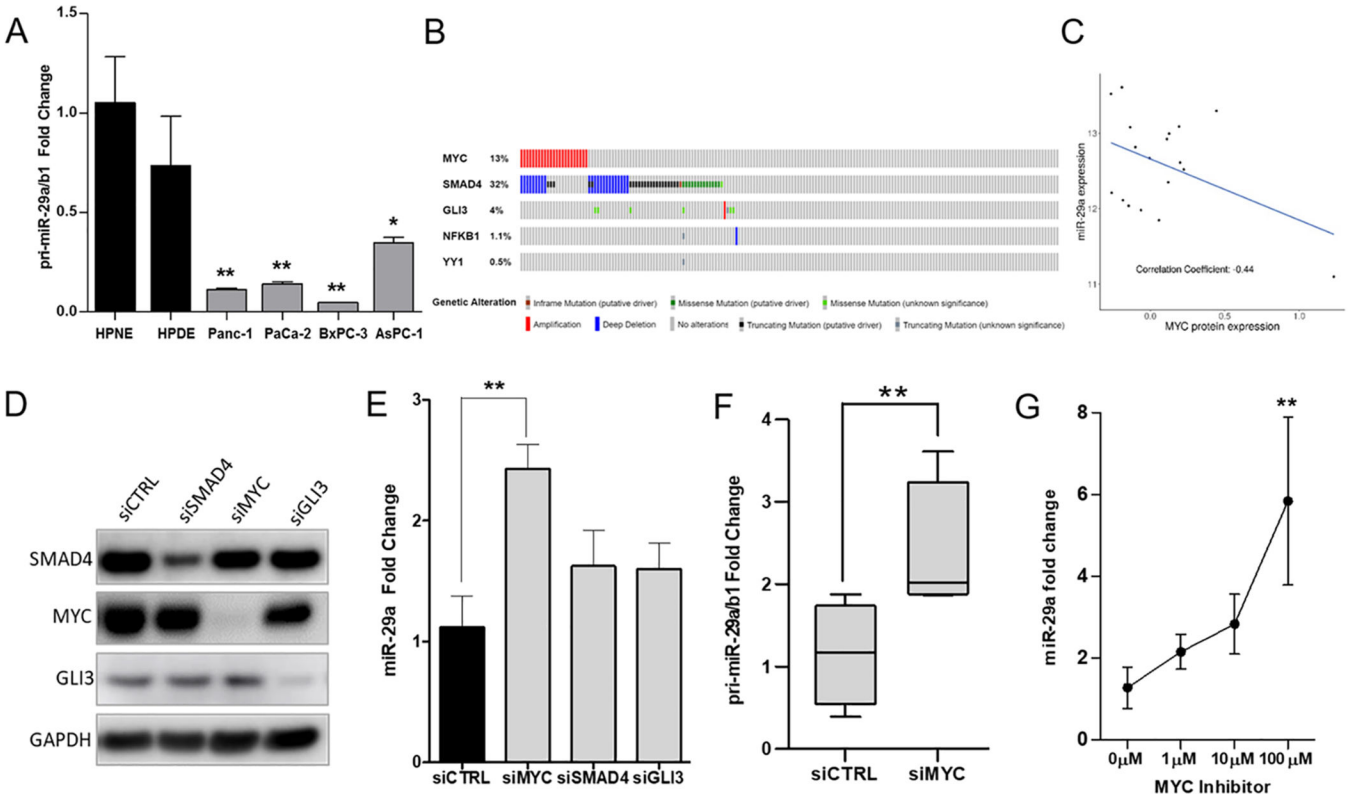

Figure 1: Knockdown/ inhibition of MYC results in increased miR-29a expression.

(A) qPCR analysis showing pri-miR-29a/b1 expression in normal human ductal epithelial cell lines (HPNE and HPDE) and human pancreatic cancer cell lines (Panc-1, MIA PaCa-2, BxPC-3, AsPC-1); n=4. **(B)** cBioportal analysis depicting the genetic alterations in the putative pri-miR-29a/b1 promoter binding transcription factors MYC, SMAD4, GLI3, NF-κB (NF- κB1) and YY1 in pancreatic adenocarcinoma patients from the TCGA database. **(C)** Regression plot indicating negative correlation between miR-29a expression (log2 normalized+1) and MYC (z-score) in TCGA pancreatic adenocarcinoma patients with alterations in *MYC*. **(D)** Western blot analysis of Panc-1 cells transfected with siCTRL, siSMAD4, siMYC and siGLI3 and assessed for SMAD4, MYC and GLI3 with GAPDH as the loading control. **(E)** Mature miR-29a expression as observed by qPCR analysis for Panc-1 cells transfected with siCTRL, siSMAD4, siMYC and siGLI3; n=4. **(F)** qPCR analysis of total RNA from Panc-1 cells transfected with siCTRL and siMYC showing pri-miR-29a/b1 expression; n=4. **(G)** Panc-1 cells were treated with various concentrations (1 μM, 10 μM and 100 μM) of small molecule MYC inhibitor 10058-F4. Subsequently, total RNA was subjected to qPCR analysis for mature miR-29a expression levels; n=3. Numerical data are represented as average fold change (ΔΔCT) ± standard error of the mean (SEM); *p< 0.05, **p< 0.01.

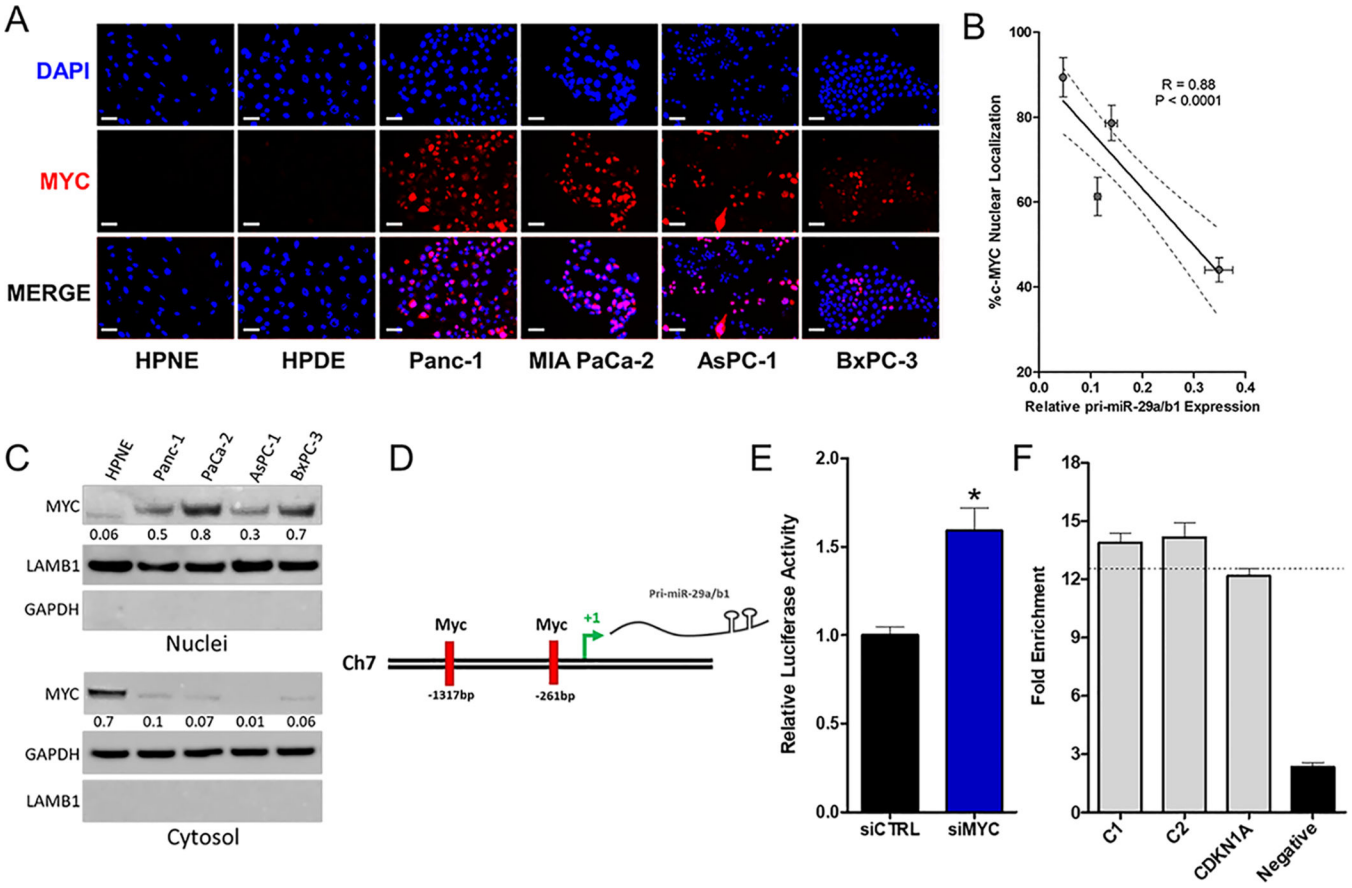

Figure 2: MYC nuclear localization negatively correlates with miR-29a and represses miR-29a by directly binding to the promoter region of the molecule in PDAC.

(A) Representative images for immunofluorescence (IF) staining of normal human ductal epithelial cell lines (HPNE and HPDE) and human pancreatic cancer cell lines (Panc-1, MIA PaCa-2, BxPC-3, AsPC-1) for MYC. Scale bar is 50 μm, 20X magnification. **(B)** Average percentage of nuclear co-localization plotted for relative pri-miR-29a/b1 expression for the cell lines presented as ± SEM; n=4. Co-localization was calculated based on DAPI nuclear staining and MYC IF. **(C)** Western blot analysis of MYC expression in nuclear and cytoplasmic fractions of HPNE, Panc-1, MIA PaCa-2, BxPC-3, AsPC-1 cell lines. Quantification of band intensities were normalized to LAMB1 for nuclear and GAPDH for cytosolic fractions respectively. **(D)** Schematic representation of the two MYC binding sites at the pri-miR-29a/b1 promoter region. **(E)** Luciferase reporter constructs containing miR-29a/b1 promoter region with MYC binding sites were co-transfected in Panc-1 cells with siCTRL or siMYC and renilla luciferase expression plasmid. All readouts were normalized to renilla luciferase activity and average relative luminescence normalized to respective controls is presented as ± SEM; n= 5, *p< 0.05. **(F)** Real-time PCR analysis of DNA fragments precipitated in a CHIP assay using Panc-1 cell line. Two primer pairs (C1 and C2) designed within conserved MYC binding sites at miR-29a/b1 promoter and a primer pair for a validated MYC-binding region of *CDKN1A* were used to detect MYC- specific binding. Fold enrichment is represented as the signal obtained for MYC immunoprecipitation relative to that with IgG. Data presented as ± SEM; n= 3.

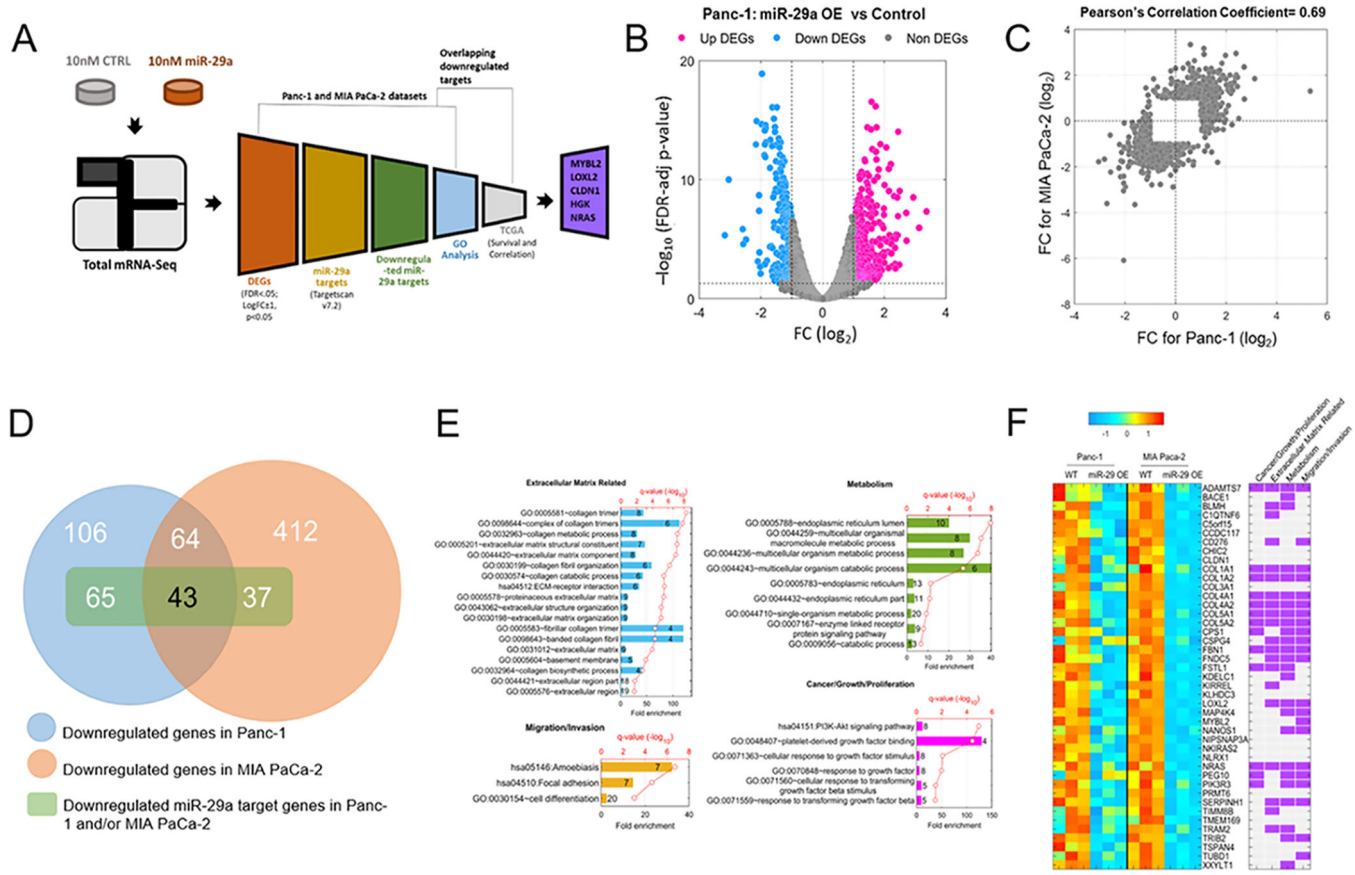

Figure 3: RNA-seq analysis and identification of differentially expressed miR-29a target transcripts from the Panc-1 and MIA PaCa-2 datasets.

(A) Schematic representation of the RNA-seq analysis pipeline used to identify differentially expressed miR-29a target genes from the Panc-1 and MIA PaCa-2 datasets. **(B)** Volcano plot depicting the differentially expressed genes obtained from RNA-seq analysis for miR-29a overexpressing (OE) and control Panc-1 cells. **(C)** Correlation between differential expression (log_2FC) of the transcripts identified by RNA-seq in the two different PDAC cell lines of Panc-1 and MIA PaCa-2. **(D)** Venn diagram of downregulated transcripts in Panc-1 and/or MIA PaCa-2 datasets. Genes with logFC < 1, FDR<0.05 and p< 0.05 were only included. **(E)** The most enriched biological processes (GO terms) for the four ontologies (ECM Matrix Related, Metabolism, Migration/ Invasion or Cancer/Growth/Proliferation) associated with the overlapping miR-29a downregulated targets identified by RNA-seq are shown. The number on or outside each horizontal axis represents the gene number for a particular GO term. The false discovery rate value is shown as q-value for each GO. **(F)** Heatmap of the 43 overlapping downregulated miR-29a targets alongside the four associated GO categories.

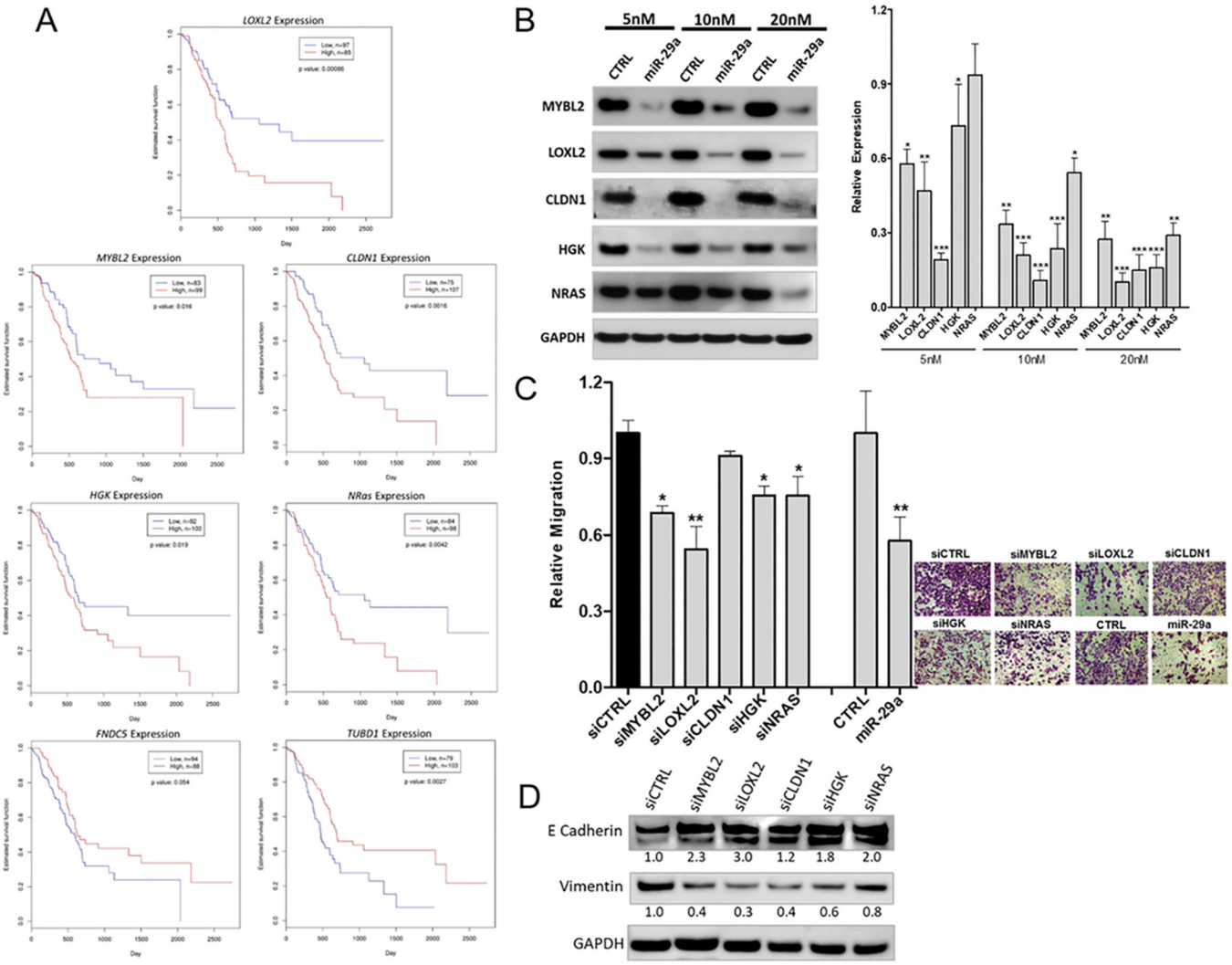

Figure 4: Functional validation of miR-29a downstream targets.

(A) Kaplan-Meier plots assessing the correlations between the seven miR-29a candidate gene (MYBL2, LOXL2, CLDN1, HGK, NRAS, FNDC5, and TUBD1) expressions and overall survival of TCGA pancreatic adenocarcinoma patients. **(B)** Panc-1 cells were transfected with different concentrations (5nM, 10nM and 20nM) of control (CTRL) or miR-29a mimics. Total protein was harvested from the cells 48 hrs post-transfection and subjected to western blot analysis for miR-29a candidate targets of MYBL2, LOXL2, CLDN1, HGK, and NRAS. GAPDH was used as the loading control. Quantification of band intensities normalized to GAPDH and relative to respective controls are represented as ± SEM; n=3, *p< 0.05, **p< 0.01, ***p< 0.001 (right). **(C)** Migration capacity of Panc-1 cells transfected with siCTRL, siMYBL2, siLOXL2, siCLDN1, siHGK, and siNRAS, or CTRL and miR-29a mimic were assessed by transmembrane cell migration assays. Relative cell migration was determined by the average number of migrated cells normalized to control (siCTRL and CTRL respectively) per 5 random fields and the data is presented as ± SEM; n=3, *p< 0.05, **p< 0.01, ***p< 0.001. **(D)** Total protein from Panc-1 cells transfected with siCTRL, siMYBL2, siLOXL2, siCLDN1, siHGK, and siNRAS, or CTRL and miR-29a

mimic were subjected to western blot analysis for E-cadherin and vimentin. GAPDH was used as the loading control.

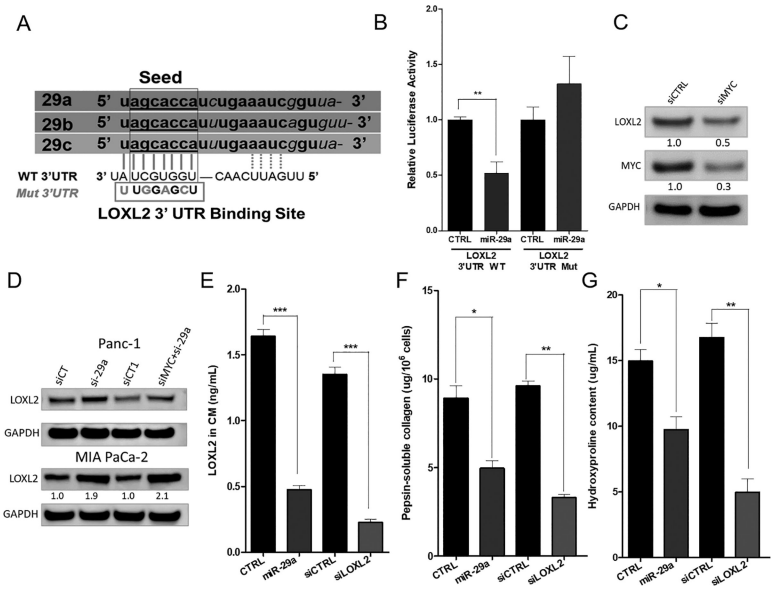

Figure 5: miR-29a directly downregulates LOXL2 in PDAC cell lines.

(A) Schematic representation of putative wild-type (WT) and mutated (Mut) binding sites of the miR-29 family members at the 3'-UTR region of LOXL2 used in luciferase assay. **(B)** Relative luciferase activity of LOXL2 3'-UTR WT and Mut reporter constructs co-transfected with control (CTRL) or miR-29a mimics in Panc-1 cells. All readouts were normalized to renilla luciferase activity for each well, and average relative luminescence normalized to respective controls is presented as ± SEM; n= 6, **p< 0.01. **(C)** Western Blot for LOXL2 and MYC in Panc-1 cells transfected with siCTRL or siMYC. Relative protein levels were measured and normalized to GAPDH levels (indicated below). **(D)** Panc-1 and MIA PaCa-2 cells were transfected with LNA miRNA inhibitor control (siCT) or LNA miR-29a inhibitor (si-29a), and co-transfected with siCT and siCTRL (siCT1), or siMYC and si-29a. Total protein was subjected to western blot for LOXL2, and expression levels were normalized to GAPDH. **(E)** Panc-1 cells transfected with CTRL or miR-29a mimic, and siCTRL or siLOXL2 were cultured in serum free media for 48 hrs. Conditioned media thus obtained were subjected to ELISA for detection of secreted LOXL2. Data is presented as ± SEM; n= 4. ***p< 0.001. **(F)** Newly cross-linked pepsin-soluble collagen in ECM of Panc-1 cells transfected with CTRL or miR-29a mimic, and siCTRL and siLOXL2. Data is presented as ± SEM; n= 3. *p< 0.05; **p< 0.01 siCTRL (for siLOXL2). **(G)** Hydroxyproline content representing heavily cross-linked insoluble collagen in ECM of Panc-1 cells transfected with CTRL or miR-29a mimic, and siCTRL or siLOXL2. Data is presented as ± SEM; n= 3. *p< 0.05; **p< 0.01.

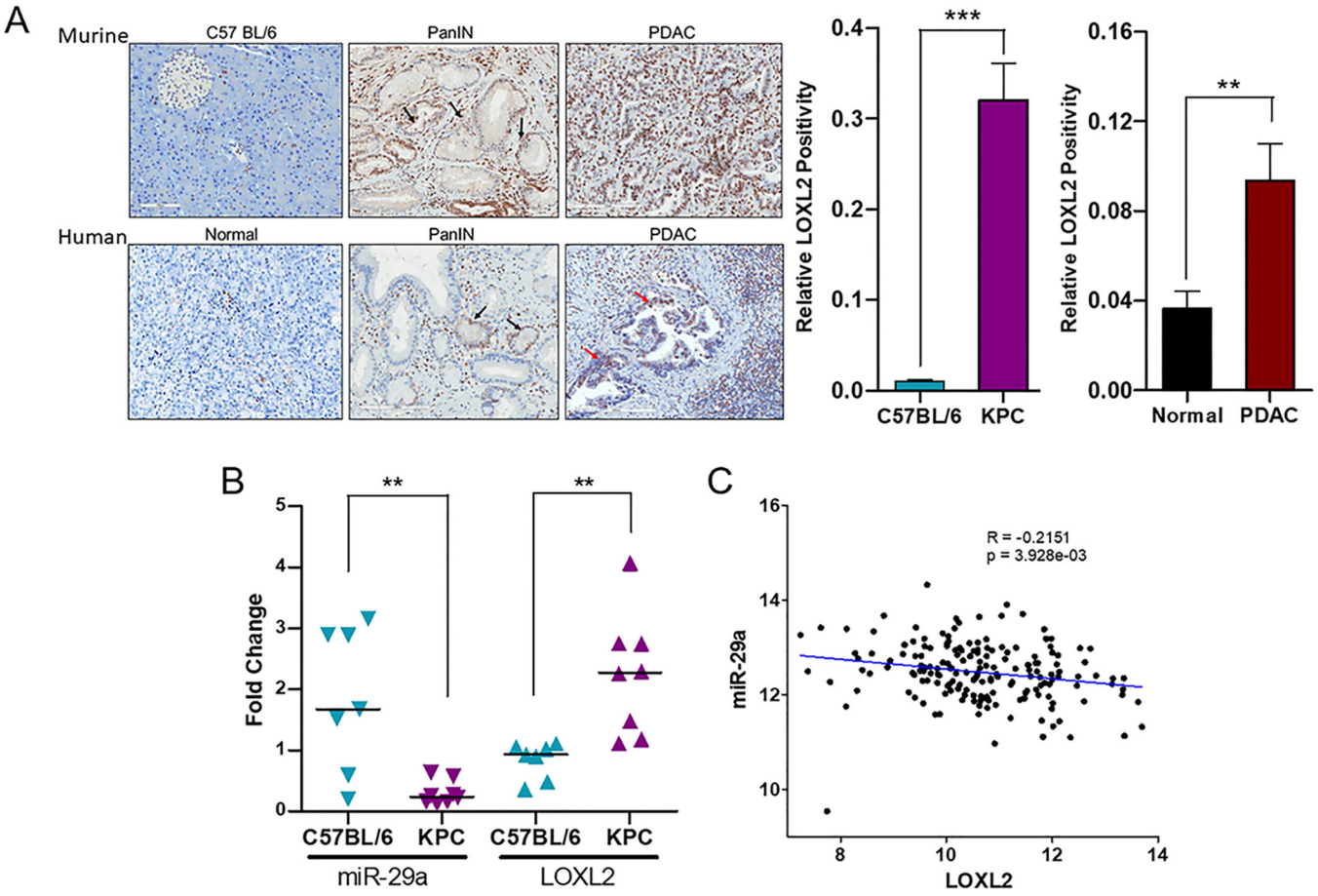

Figure 6: Elevated LOXL2 levels inversely associate with miR-29a expression in KPC mice pancreas and human PDAC tumors.

(A) *Upper panel*: Representative photographs for immunohistochemical staining of LOXL2 in pancreatic sections from control C57BL/6, and $Kras^{LSL.G12D/+}$; $p53^{R172H/+}$; Pdx1-Cre (KPC) mice at 4.5– 6 months of age (original magnification X20). While negative staining was observed for control C57BL/6, KPC mice pancreata with PanIN lesions (black arrows) and PDAC stained positive for LOXL2 with significantly higher LOXL2 expression. LOXL2 positivity from immunohistochemistry analysis was quantified and presented as ± SEM; n= 15 animals per group (right), ***p< 0.001. *Lower panel*: Representative photographs for immunohistochemical staining of LOXL2 in PDAC clinical specimens. Positive staining for LOXL2 was observed around PanIN (black arrows) and PDAC (red arrows) lesions in PDAC tumor specimens with little or no staining for normal patient pancreatic specimens. LOXL2 positivity was quantified and presented as ± SEM (right); n= 6 for normal controls and n= 4 for patient PDAC tumors, **p< 0.01. **(B)** Total RNA from frozen pancreatic tissue sections of C57BL/6 (n=7; solid blue) or KPC mice (n=8; solid purple) were isolated and subjected to qPCR analysis to determine miR-29a and LOXL2 expressions. miR-29a expression is represented by inverse triangles and LOXL2 expression is represented by triangles. Mean expressions of miR-29a and LOXL2 for each group are indicated as horizontal lines, **p<

0.01. **(C)** Correlation analysis between LOXL2 and miR-29a expressions in PDAC patients from the TCGA database (n= 178).

Table 1:

miR-29a candidate targets identified from RNA-seq analysis in PDAC cells.

Gene Symbol	Gene Name	RNA-seq-Fold Change in miR-29a OE PCCs (log 10 ratio)		Cox Regression Coefficient TCGA-data
		Panc-1	MIA PaCa-2	
*MYBL2/b-myb**	MYB proto-oncogene like 2	−1.986	−2.869	0.287
*LOXL2**	Lysyl oxidase like 2	−2.053	−2.415	0.229
FNDC5	Fibronectin type III domain containing 5	−2.159	−1.753	−0.212
*CLDN1**	Claudin 1	−1.246	−1.684	0.402
*MAP4K4/ HGK**	Mitogen-activated protein kinase kinase kinase kinase 4	−1.265	−1.494	0.302
*NRAS**	NRAS proto-oncogene, GTPase	−1.428	−1.135	0.354
TUBD1	Tubulin delta 1	−1.199	−1.223	−0.253

* indicates final candidate genes validated by functional assays in our study